Volume 1 | Number 1 | Jan 2013 | Pages 1–100

PCCP

Physical Chemistry Chemical Physics
www.rsc.org/pccp

ROYAL SOCIETY OF CHEMISTRY

ROYAL SOCIETY OF CHEMISTRY

www.rsc.org/pccp

ARTICLE

Molecular basis of substrate translocation through outer membrane channel OprD of *Pseudomonas aeruginosa*

Susruta Samanta,[a] Andrea Scorciapino,[b] and Matteo Ceccarelli[a*]

The objective of this study is to identify the structural features governing the transport of molecules through nanometric channel proteins at a molecular level. Our focus is to come up with a precise understanding of the structure and dynamics of the outer membrane porin OprD of the Gram-negative bacterium *Pseudomonas aeruginosa* by studying translocation of natural amino acid residues/substrates 10 through it. We used in-silico electrophysiology and metadynamics simulation techniques as they can provide precise information on the molecule/channel interactions at the atomic scale that allow testing quantitative structure-function relationships. We performed our simulations on the whole OprD protein, with all loops modelled and without any constraints to keep the channel open. Dynamics of both internal and external loops and the polar nature of the eyelet region play important role in modulating 15 translocation of molecules through OprD by creating two alternative paths for translocation. All positive residues take the main path upon binding in the negative pocket just above the constriction region. The same factor is unfavourable for negative substrates and hence they have relatively higher barrier for translocation. Differently, neutral substrates do not show any specificity and they can follow the two alternative paths.

20 .

Introduction.

Pseudomonas aeruginosa (PA) is a significant cause of nosocomial pneumonia and it is the most prevalent pathogen found in patients with severe injury or burns, where the 25 associated mortality rate is up to 50%.[1,2] Due to its poorly permeable outer membrane, PA shows strong resistance to a wide range of antibiotics. In some bacterial species, relatively large general diffusion porins (like OmpF and OmpC in *E. coli*) are expressed and used by polar antibiotics to penetrate the cell.[3] PA 30 lacks these large pores and instead, has many specific channels, (like OprD) which allow the uptake of small natural substrates like arginine.[4,5] Although their specificity, these channels are considered to be potential entry points for polar antibiotics. Interestingly, the lack of large pores correlates with a high 35 resistance level of PA.

A way to increase the efficacy of antibiotics acting against Gram negative bacteria would be to enhance their permeation through the outer membrane, for example by finding some specificity for one or more pores.[6] However, the question of 40 whether there exists any specificity for translocation through these channels still remains unanswered.[6,7] This is mainly because of the lack of a robust and reliable experimental method to measure permeability.[8] Recently, electrophysiology experiments combined with simulations showed some specificity

45 for zwitterionic molecules through general diffusion porins.[9] However, the exact definition and the extent of specificity, if any, still remains an open question, especially for specific channels like OprD.

PA OprD is considered the main entry point for antibiotics of 50 the carbapenem family (e.g., imipenem, meropenem, doripenem etc.). They show excellent activity against PA because of their high stability to the chromosomally encoded AmpC β-lactamase produced by this species.[10] Some basic amino acids and small peptides containing these amino acids are also natural substrates 55 for OprD.[11,12] As mentioned earlier, till date, there is no experimental evidence for the presence of a specific binding site for any of them within the OprD channel.[13] There were only some suggestions that there might be some binding sites involved in imipenem translocation.[11] Recent simulation studies of Parkin et 60 al. suggest that translocation of arginine happens as a result of a series of binding sites and the motion of the backbone in the eyelet region is conserved.[14,15] However, the mechanism of transport and the interior architecture of the OprD channel are yet to be properly understood.

65 OprD is no longer considered strategic for developing new antibiotics, because it is under-expressed in almost all PA pathogen strains. Instead, it is being represented as a useful model for the development of antibiotics of the carbapenem family. Many experimental data are available in this direction of 70 research.[5,16-18] In addition, OprD belongs to a large family of

channels – OccD and OccK from PA and their orthologs from *Acinetobacter baumanii* (AB). Hence it will be specifically helpful to use OprD as a model for testing transport properties in PA and AB. Understanding structure dynamics of OprD, its key chemico-physical features and interactions with natural substrates will help us to understand a large spectrum of porins by setting up a benchmark and this will initiate huge possibilities for further research.[19-21]
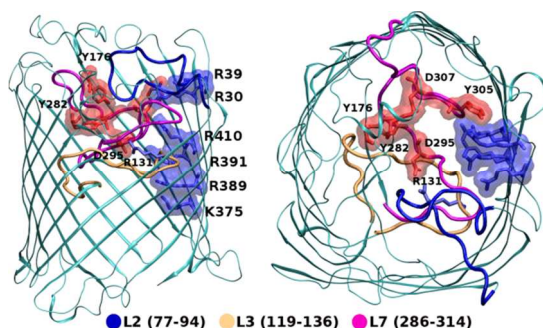
Fig. 1 The structure of OprD. The important loops, the basic ladder and the negative pocket are shown.

In this work, we aim towards proposing the detailed architecture for the OprD channel by explaining the mechanism of transport of ions and small molecules in more details, starting from natural substrates. We expect the finding would be advantageous to recognise the reason for specificity and affinity for certain type of molecules, necessary in a near future to define some rules for designing antibiotics with enhanced permeation. We studied channel conductance to understand the dynamics of the flexible loops in OprD with the aim to identify and characterize the open and closed states of this porin. We investigated the translocation of a wide range of positive, negative, and neutral substrates to find out how the electrostatics of a molecule affect the process of translocation through OprD. The present study suggests that the dynamics of the internal loops (L3 and L7) near the constriction region and their interaction with the external ones (L2, L6. L8) play a pivotal role in transport of substrates through OprD. This is influenced by the electrostatic effect of the basic ladder (comprising arginine and lysine residues) and negatively charged residues near the constriction region of OprD.

Methods.

Simulation details:

The starting structure for the channels were prepared following a protocol as described earlier[22], with the porin embedded in a POPC (1-palmitoyl-2-oleoyl-sn-glycero-3-phosphocholine) lipid bilayer consisting of 238 lipid molecules and solvated with ~15000 water molecules. We used the improved crystal structure (PDB code 3SY7) which was resolved at a resolution of 2.15 Å.[16] The loop L2 (residue index 77-94), parts of loop L4 (residue index 159-179) and loop L7 (residue index 287-290) were missing in the crystal structure. Thus, we modelled the missing residues with the program Modeller.[23] The structure of OprD along with important loops and residues is shown in Figure 1. We used the Amber99sb-ildn forcefield parameter for OprD, General

Amber Force Field (GAFFlipid) for POPC, and TIP3P model for water.[24-26] We performed unconstrained MD simulations with the AceMD program.[27] We simulated a periodic box in the NVT ensemble using the Langevin thermostat (300 K) and the particle mesh Ewald (PME) scheme with fourth order splines and 9Å cut-off for electrostatic interactions.[28]

System preparation

The protein was embedded in pre-equilibrated POPC bilayer and overlapping chains were deleted. The lipid headgroups were restrained along z-axis (allowing movement along XY plane) and the system was equilibrated to fill in the gaps. Water molecules were added. The water molecules trapped in protein-membrane interface and inside the channel were eliminated. The system was equilibrated with restrain on the C_α and C_β atoms. Because the system might need a different rearrangement along the XY plane and the Z direction, we performed different equilibration steps in the NPT ensemble. We performed short runs (100 ps) using fully flexible cell (X, Y and Z box sides can change independently), followed by a longer run (1 ns) with isotropic changes along the three directions. If along the isotropic runs strain is accumulated more in one direction than in others, this is corrected by the anisotropic runs. After a long (10 ns) NPT equilibration using the isotropic barostat, starting from the last step we switched to the more stable NVT algorithm for metadynamics production runs, as the addition of a bias can easily perturb the stability of the NPT algorithm.

Mutations:

In addition to the wild type OprD, we selected five mutants – a point mutation at the eyelet region, partial deletion of an internal loop and deletion/mutation of two external loops. The mutations involving internal regions are R131G and DL3 (Residues 130 to 135 of loop L3 replaced with two glycines), for which experimental data on conductance are available. Further, we prepared the DL6 mutant (residues 241-EGKAKAGD-248 in loop L6 removed), and following Huang et al[13] and Epp et al[29] two DL8 mutants that would enhance meropenem uptake. In the mutation proposed by Huang et al, part of an external loop L8 was deleted (deletion of 349-MSDNNVGY-356 from L8). In the mutation proposed by Epp et al, 349-MSDNNVGYKNYGY-361 was substituted with V-DSSSSYAGL-Y in loop L8. In this article, this mutation has been denoted as DL8*. The locations of all the mutations are shown in Figure S1 in the SI.

Chemical environment and ion conduction simulations:

All the simulations were run at 0.3M KCl solutions. Selected systems were run in two pH conditions – pH 7, and pH 5. To achieve the desired pH, pKa values of all the residues were calculated using the PROPKA server and the protonation state of residues appropriately modified.[30] The residues protonated to achieve pH=5 are D90, D185, D281, D307, and H367.

In order to investigate ion conduction we applied an external electric field using the in-built plugin in AceMD. Here a constant force is applied at each atom in the system having a point charge. In our simulations, the external electric field corresponds to an applied potential of 1 V. Though this value is 5 to 10 times higher than the values applied in typical experimental setup, it ensures to evaluate the conductivity in the time range spanned by molecular

dynamics simulations, i.e. hundreds of nanoseconds.

Cluster analysis and principal component analysis:

We performed cluster analysis using the GROMOS clustering algorithm which is based on the root-mean square deviation (RMSD) cut-off.[31] The conformation with the least deviation from other members of the cluster is used as the representative structure of the clusters. A RMSD cut-off of 1.5 Å and 2.0 Å was used to determine neighbouring backbone atoms conformation of wild type OprD at pH 7 and 5, respectively. Structures were sampled every 10 ps for the analysis.

A principal component analysis was performed to identify functionally relevant motions in OprD.[32, 33] The backbone atoms of wild type OprD were used to explore the conformational subspace at pH 7 and 5. Details of this method can be found elsewhere.[34]

Metadynamics:

Substrates permeation was investigated through metadynamics simulations as implemented in the Plumed 1.3 plug-in[35] within the AceMD software.[27] We applied the Well-Tempered metadynamics protocol where the Gaussian weight factor is periodically rescaled providing a convergence parameter to monitor during the metadynamics simulation.[36] An initial bias with the Gaussian height of 1.2 kcal was added every 2 ps (with $\Delta T=3000K$). All the metadynamics simulations were run at neutral pH.

We selected two geometric collective variables to bias in order to sample the porin-substrate interactions. The reference is the axis of diffusion, labelled as Z: (1) the orientation of the substrate with respect to Z (Z_{theta}) and (2) the projection along Z of the center of mass of the antibiotics with respect to the center of mass of the porin (Z_{cm}). To ensure that substrates stay inside the porin for the entire course of simulation, we set two potential walls at +25 Å and -16 Å for Z_{cm}, respectively, covering the whole pore. In our simulations, positive value of Z_{cm} indicates the extracellular side, and negative value indicates the periplasmic side. Initially we placed the substrate molecule on the extracellular side of OprD at least 20 Å away from the constriction region. The coordinates we selected are general enough to allow the comparison of different substrates. In addition, we did not force substrates either to follow a particular path during permeation, for example by biasing the opening of the constriction region, or to visit any pre-defined binding/affinity site, for example by biasing the interaction with selected protein residues.

The convergence of a metadynamics run depends on complete sampling of the porin-substrate conformational space which is computationally very expensive to achieve with a single run. For this reason, we constructed the final free energy surface using the 'multiple walkers' method.[37] In the multiple-walkers algorithm, several metadynamics simulations (walkers) are performed at the same time. Each walker adds its own biases, but it also reads those added by the other walkers, thus accelerating the sampling of the whole space. After obtaining the first translocation, we prepared 5 systems where the initial position of the substrate ranged throughout the length of the whole OprD and ran them independently (with the same parameters for the metadynamics simulation). All the free energy surfaces are result of at least 1 μs

of simulation time. Within this time the convergence parameter, the Gaussian height, arrived to a baseline below the 1/100 of the initial value (Figure S13 in the SI). In addition, to assess the convergence of our free energy surfaces we compared them with the one reconstructed 50 and 100 ns before the total time, obtaining differences lower than 1 kcal/mol (Figure S14 in the SI).

Table 1 Calculated conductance value for the systems simulated for 300 ns at 0.3M KCl concentration.

System	pH	HC (pS)[a]	LC (pS)[b]	Expt (pS)	Cl⁻/K⁺ Ratio
WT	7	316.2	16.7	28	0.26
	5	434.6	23.2	-	0.52
R131G	7	-	32.8	44	0.08
	5	271.5	65.2	-	0.88
DL3	7	770.0	-	-	0.26
	7[c]	-	74.8	88	0.04
	5	1194.0	-	-	0.61
DL6	7	254.0	29.0	-	0.11
DL8	7	530.6	40.9	-	0.14
DL8*	7	311.4	35.5	-	0.19

[a]HC = high conductance state, [b]LC = low conductance state. [c]300 ns simulation with closed loop L2. Experimental data from Biswas et al.[16] The last column represents the ratio of the number of chloride and potassium ions passed through the constriction region during 300ns of simulation.

Results and Discussions.

Simulations with external electric field:

The primary goal of this investigation is to understand the structure elements of the OprD channel by studying the ions conductance. To test our set-up we compared the calculated conductivity with the (few) experimental data available, namely for the wild type (WT), the mutations R131G and DL3 (Table 1). They are in fair agreement. Although the absolute values of conductance were slightly underestimated in our simulations, trend and slope were well reproduced.
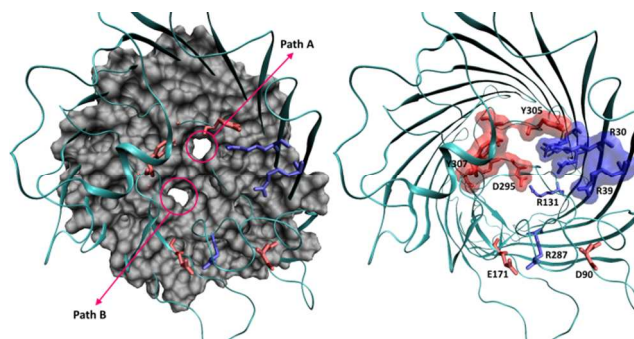
Fig. 2 Paths of translocation through OprD.

Wild type OprD at pH 7.

For each system the conductance increased with decreasing pH. For the WT at pH 7, three conductance states are seen (Figure S2). The low conductance state (16.7 pS) is very short lived and followed by a medium (114 pS) and higher conductance state (316 pS). The interplay between the internal loops L3 and L7 (which constitute the constriction region) is the major contribution to this effect. There are two possible paths of translocation through OprD. These paths are shown in Figure 2.

Path A is polar in nature as it lies between the basic ladder and the negative pocket (Y176, Y282, D307, Y305, D295). Path A is controlled by the fluctuations of loop L7 internally and L2 externally. Path B is relatively narrower and controlled by the salt
5 bridge interaction between R131 (in L3) and D295 (in L7) (and by L6 and L8 externally, as shown here). In order to open Path B, this salt bridge has to be broken. Then, R131 side chain can flip and take part in a new salt bridge interaction occurring externally with D90 (in L2). In Figure S3 in the SI, both these two salt
10 bridges involving R131 are shown.
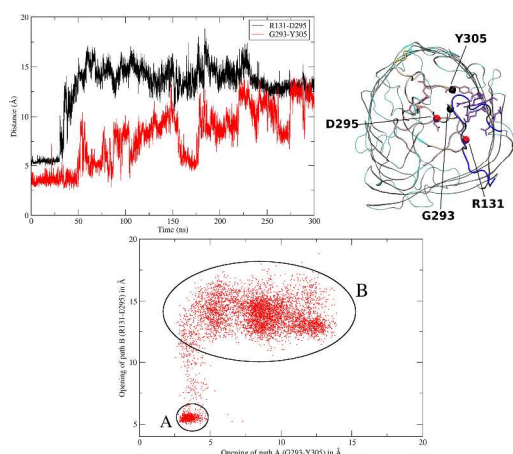
Fig. 3 a) Distance between R131-D295 and G293-Y305 (top-left); b) position of the residues (top-right); c) relative relation between them (in WT at pH 7).
15

In Figure 3, the interplay between path A and B is described. We have quantified the opening of path A with the distance between the center of masses of G293 and Y305. The opening of path B has been quantified with the distance between the center
20 of masses of R131 and D295. Initially both the paths are closed, corresponding to the low conductance state. After 35 ns, the R131-D295 interaction is broken and the conductance increases. The distance between G293 and Y305 keeps on increasing throughout the course of the simulation indicating opening of
25 path A. In the relative relation between them, the close state (A) and the open state (B) are very well defined with the selected distances.
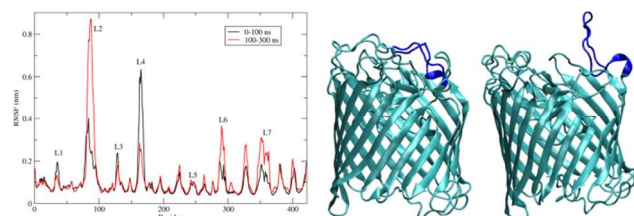
Fig. 4 a) Comparison of the residues RMSF for the WT OprD at pH 5
30 calculated for the low conductance state (0-100 ns) and high conductance state (100-200 ns). b) Representative structure of the OprD during the low conductance state (left) and the high conductance state (right) at pH 5. The loop L2 is shown in blue.

Wild type OprD at pH 5.

35 At pH 5, both the open and closed states show higher conductance with respect to neutral pH. The current-voltage characteristic or the I-V curves in Figure S2 show a low

conductance state till 100 ns (23.2 pS) and then a consistent increase in conductance (434.6 pS). The two conductance states
40 are modulated by the dynamics of the external loop L2, which seats like a flap at the mouth of OprD. Figure 4a shows the comparison between the RMSF per residue for the first 100 ns of simulation (low conductance state) and the last 200 ns of simulation (high conductance state) at pH 5. As expected, major
45 fluctuations around the loop regions were found. Major differences were observed for L2 (77-94) and L4 (159-179). The loop L2 shows much larger fluctuation during the second half of the simulation, which corresponds to the high conductance state. Exactly opposite trend is seen for the loop L4 which is more
50 stable in the high conductance state.
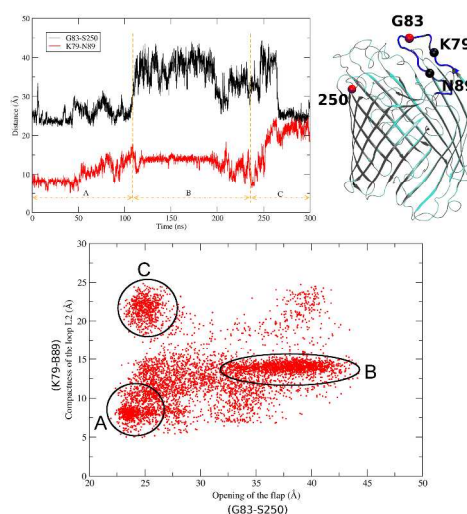
Fig. 5 a) Distance between K79-N89 and G83-S250 (top-left); b) position of the residues (top-right); c) relative relation between them (in WT at pH5).
55

Loop L4 is an external loop and it does not seem to have major contribution towards the ion transport through OprD. We focused on the behaviour of loop L2 which is also an external loop but it works like a flap, which may open/close the mouth of path A.
60 Figure 4b shows a representative structure for both the conductance states. The loop L2 has been highlighted in the figure showing its clear contribution. The figure shows that the loop L2 can close the channel resulting in the low conductance state. To better characterize the dynamics of the L2, we
65 investigated its compactness (represented by the internal distance K79-N89), and the opening flap-like movement (represented by the distance between G83-S250). Details are shown in Figure 5. The figure shows that during the low conductance state (<110ns) both the distances are short, meaning that the loop L2 is compact
70 and the flap is closed (state A in Figure 5). After 110 ns, the flap opens up (longer distance between G83-S250) and stay in such state till ~270 ns (state B in Figure 5). Interestingly, despite the flap closes again towards the end of the simulation, as seen in the IV curve the conductance is not significantly affected. This is
75 because the distance between K79-N89 becomes even larger, resulting in a lower compactness of the loop thus allowing ions pass through it (state C in Figure 5). In the same figure, the relative relation between the selected distances has been plotted to quantify the different states shown with black circles.
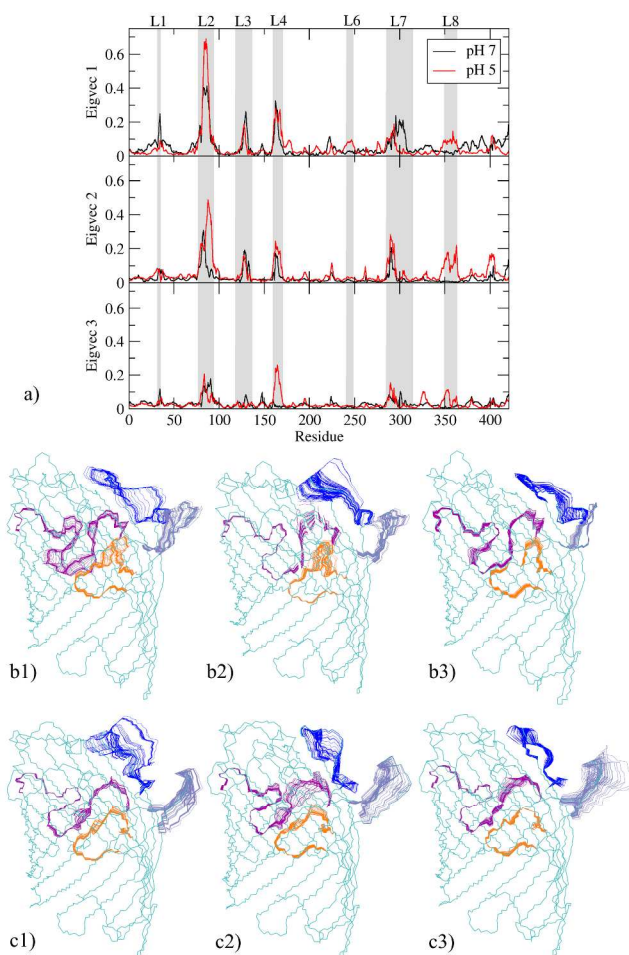
Fig. 6 a) Representation of the RMSF of the backbone atoms along the first three eigenvectors at pH 7 (black) and pH 5 (red); Major fluctuations on the loop regions corresponding to the first three eigenvectors are shown for pH 7 in the upper panel (b1, b2, b3) and pH 5 (c1, c2, c3) in the bottom panel. Colour codes for the loops: blue for L2, grey for L4, orange for L3, purple for L7.

Principal Component and Cluster Analysis.

From these observations it is clear that the relative motions of the loops play very crucial role in the translocation process through OprD. We performed principal component analysis (PCA, also known as essential dynamics) to resolve the most relevant motions in OprD. The first 10 eigenvectors account for 72% and 80% of the cumulative relative positional fluctuations (RPF) for pH 7 and 5 respectively. Among them, the first three eigenvectors contribute 35%, 10.2%, and 6.4% at pH 7; at pH 5 they contribute 30.9%, 24.9%, and 6.8%. Analysing these three eigenvectors would allow us to understand the major structural fluctuations in OprD. Figure 6 shows RMSF of the backbone atoms in the first three eigenvectors at pH 7 and 5. Their corresponding structures are reported in the same figure. It is evident that loops L2, L3, L4 and L7 account for the major fluctuations in all the simulations. The motion of external loop L1 and L4 (shown in grey) does not affect the opening of the porin. The effect of loop L2 was mentioned earlier in detail. The PCA analysis shows us this is indeed the most determining factor responsible for opening and closing of the channel. At pH 5, the flap motion accounts for the most relevant motion (Fig 6c1). This motion is very important,

but not the most contributing factor at pH 7. At pH 7, the widening of the loop is the most prevalent motion.

We performed cluster analysis to pinpoint the most representative structures and they are shown in Figure 7 for both pH conditions. We observed a total of 9 clusters at pH 7, and 5 clusters at pH 5. The first cluster contributes 35% at pH 7 and 28.3% in pH 5. The second cluster represents 43.3% at pH 7, and 35% of the total population at pH 5. At pH 5, the most prevalent cluster corresponds to an open structure of OprD. The second most populated structure at pH 5 corresponds to a semi-open structure. At pH 7, two most prevalent structures corresponds to semi-open state of OprD. This elucidates the reason for higher conductivity of OprD at lower pH. We mentioned earlier that at pH 5, D90, a residue in loop L2 is protonated, rendering it incapable of salt-bridge interaction with R131 (Figure S3 in the SI). This increases the mobility of loop L2 at pH 5.
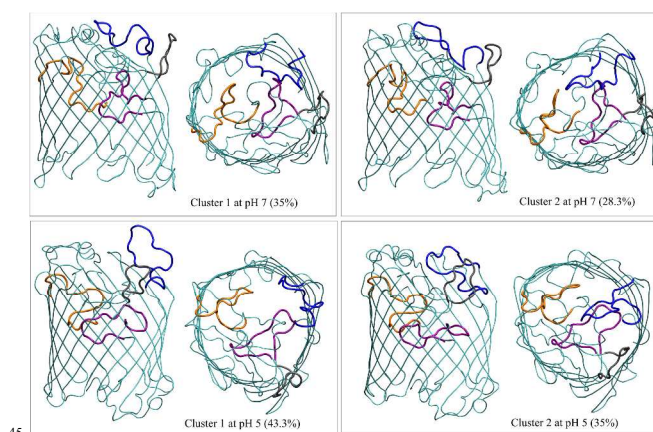
Fig. 7 The two most representative structures of OprD at pH 7 (top) and pH 5 (bottom).

R131G Mutation.

In R131G mutation, the R131-D295 salt bridge is suppressed as well the interaction R131 with loop L2. As consequence path B is open for the whole simulation and no important movement of L2 is observed. In addition, replacement of arginine with a glycine results in a small increase in available area at the constriction region as seen in Figure 8. Indeed, the low conductance state of the mutant (32.8 pS) has higher conductance that the WT porin. This is in a good agreement with the experimental value at pH 7.[16] The loop L2 stayed in the close state for the whole course of simulation and hence, we did not see a high conductance/open state. At pH 5, before the loop L2 in the R131G mutant opened up, and we observed the high conductance/open state.

DL3 Mutation.

The experimental work by van den Berg et al. on the mutation DL3 resulted in conductance of 88 pS.[16] In this mutation, 6 residues (S130, R131, L132, F133, P134, and Q135) from the loop L3 were replaced by two glycine residues resulting in a significant increase in the available area at the constriction region (Figure 8). Our simulations showed a remarkably high conductance both at pH 7 (770 pS) and pH 5 (1194 pS). In both the cases, the loop L2 was found in the open position. In order to further confirm the position of the loop L2 as one of the most important factors controlling the conductance of ions through

OprD, we chose a conformation corresponding to the close state. To keep L2 in this closed state we restrained the Cα atoms for the whole course of simulation. Conductance was found as low as 62.4 pS. This is in fair agreement with the experiments and

[5] further supports our finding that dynamics of the loop L2 is probably the most important factor governing ions translocation through OprD channel.
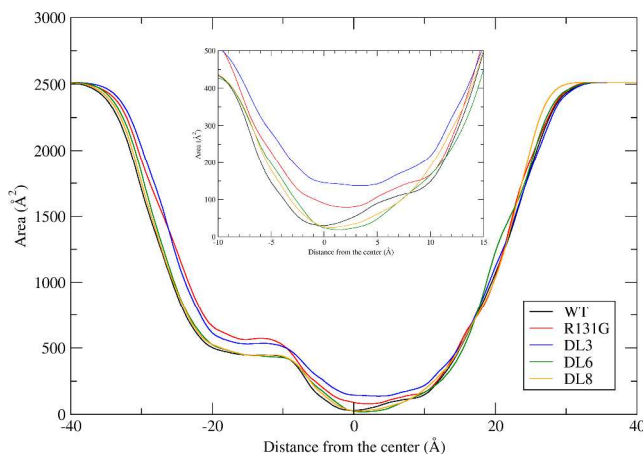
Fig. 8 Comparison of the available area in the porin at pH 7.

[10] **External Loops Mutations.**

Apart from loop L2, there are two other interesting loops on the periplasmic side of the porin, loops L6 and L8. The latter, in particular, has been reported to have significant effect on translocation of antibiotics through OprD.[13, 29] To understand the

[15] effect of these loops, we simulated three appropriate mutants: DL6, DL8, and DL8*. All of these mutations showed both low and high conductance states as reported in Table 1. The conductance of these mutants in the LC state is in the same order of magnitude of the R131G mutant at neutral pH. The R131-

[20] D295 distance (Figure S5) shows that for all of the three mutants, the interaction is broken and path B is open for major part of the simulation. These loops being external, do not affect the available area at the constriction region (Figure 8).

For all the simulated systems, the number of translocated

[25] cations was higher than anions (Table 1). The translocation of anions increased only when the pH was lowered. Indeed, at pH 5, one of the residues protonated is D307, which is a member of the negative pocket above the constriction region. Cation transport of the porin is most prevalent in case of R131G, DL6, and DL8,

[30] where path B played important role because of the presence of the negative D295 residue controlling translocation through this path. For the mutant R131G such effect was foreseen, the same cannot be said for the other two mutants, thus suggesting an increased accessibility of the path B to ions upon loops deletion.

[35]

Table 2 Energy barriers for percolation of substrates through OprD. The minimal projection areas (in Å^2) of the substrates are shown in the parenthesis.

Positive		Negative		Neutral	
Lysine	10.9 (29.5)	Glu. acid	13.9 (24.3)	Histidine	19.9 (29.9)
Arginine	6.9 (30.9)	Benzoate	13.3 (23.3)	Serine	10.6 (24.2)
Ornithine	4.7 (28.5)			Leucine	8.0 (29.5)
Histidine	4.6 (27.5)			Glycine	7.4 (18.2)

^{a} The values of free energy are in kcal/mol.

[40] **Translocation of substrates through OprD:**

To identify potential binding/affinity sites inside the porin and they role in permeation, we studied the translocation of simple amino acids and small molecules through OprD. We selected four positively charged amino acids: arginine, lysine, ornithine and

[45] histidine. To investigate the effect of a net positive charge, we also simulated the neutral form of histidine. We studied two negatively charged substrates in addition: benzoate and glutamic acid. It should be noted that, apart from benzoate, all the selected amino acids have been simulated with the alpha-carboxyl group

[50] negatively charged and the alpha-amino group positively charged. Also structurally, ornithine and lysine are very similar, with lysine having an extra carbon in the chain. Glutamic acid has almost the same length but has the opposite charge at the end of the chain. In addition to neutral histidine, we have simulated three

[55] more neutral substrates - glycine, leucine, and serine. With this selection, we could investigate the effect of size and charge on the binding and translocation properties of substrates in OprD. The barriers of translocation of the substrates are shown in Table 2.

[60] It is clear that OprD is characterized by selectivity for positively charged substrates over negatively charged or neutral substrates. Even a relatively small molecule like benzoate has a higher barrier of percolation than significantly larger positive substrates. Histidine represents an extremely informative case.

[65] Despite the two simulated forms are structurally almost identical, the barrier for the neutral form is much higher than for the positively charged one.
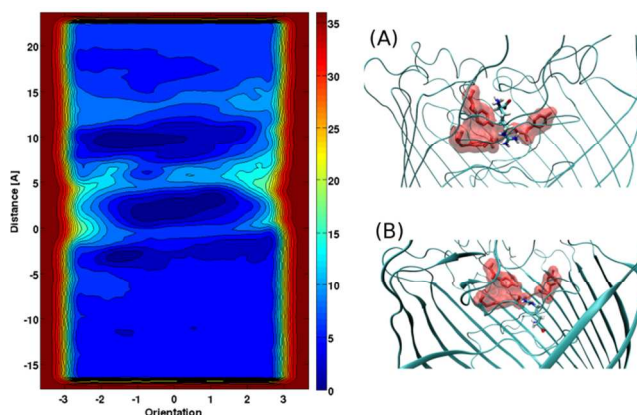
Fig. 9 FES of translocation of arginine through OprD is shown in the left.
[70] The structures corresponding to the minima in the FES of translocation of arginine through OprD (A → top, B → bottom) are shown in the right.

Translocation of positive substrates.

The reconstructed FES of translocation of arginine through OprD is shown in Figure 9. The energy barrier for the translocation was

[75] found to be 6.9 kcal/mol. The FES shows two clear minima which correspond to the presence of strong binding sites inside OprD. In the same figure, the corresponding structures to these

minima are shown. Essentially, the minimum corresponds to the same negatively charged pocket comprising residues Y176, Y282, D307, Y305, D295 and is located just above the constriction region, identified as the minimum of the pore internal radius. Arginine interacts with residues of this pocket either positive side up or down. As the FES y-axis reports the location of the centre of mass of arginine, the two orientations produce two distinct minima. Rotation of the molecule in this region corresponds to the highest barrier for translocation.
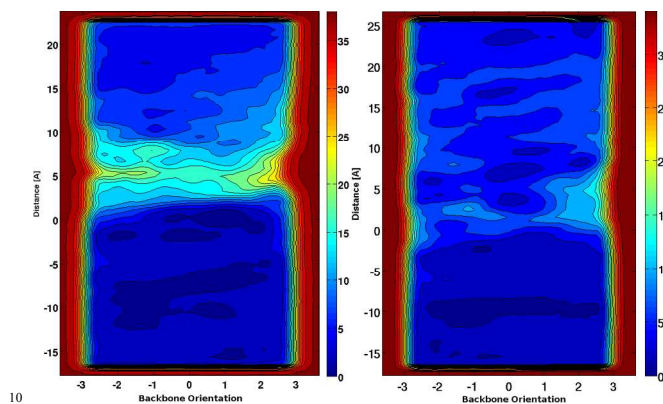
Fig. 10 FES and path of translocation of histidine through OprD. The figures in the left correspond to the neutral form and figures in the right correspond to the positively charged form.

The energy barrier for the translocation of lysine was found to be 10.9 kcal/mol and that for ornithine was 4.7 kcal/mol. The reconstructed FESs of translocation of these positively charged residues are shown in Figure S6 in the SI. Similar to arginine, prominent minima are located near the constriction region. The structures corresponding to these minima are shown in Figure S7 and S8 in the SI. The translocation of the positive substrates shows striking similarities. The polar nature of the eyelet region favours specific orientation of the zwitterionic backbone, with the carboxyl group pointing the basic ladder whereas the amine group the negative pocket. The positive amine group anchors in the negative pocket while the negative carboxyl group slides from R410 to R391 along the basic ladder. The presence of a positively charged chain facilitates anchoring in the negative pocket and molecule sliding through the eyelet region.

Translocation of Histidine (positively charged and neutral form).

The reconstructed FES of translocation of the two forms of histidine through OprD are shown in Figure 10. The energy barriers for the translocation were found to be 19.9 and 4.6 kcal/mol for the neutral and the positive form, respectively. Structurally, the molecules are almost identical. The presence of the positive charge on the imidazolium ring makes a huge difference in the energy barrier for translocation. The positive charged form favours the binding and translocation through the negative pocket, which is path A. Conversely, this path it is not energetically favourable for the neutral form that has thus to follow the path B (Figure 12).

Positive form of histidine has the minima comparable to the other positive substrates investigated and the corresponding structures are shown in Figure S9 in the SI. The neutral form lacks these minima and the same region in the FES shows the

highest barrier to translocation. In this case, the energy minima in the FES lie below the constriction region (Figure 10 and S10).

Translocation of Negative Substrates:

The reconstructed FES of translocation for negatively charged benzoate and glutamic acid through OprD are shown in Figure 11. The energy barriers for the translocation were found to be 13.3 and 13.9 kcal/mol for benzoate and glutamic acid, respectively. These values are significantly higher than those found for positively charged substrates, even in the case of a relatively small molecule like benzoate. The presence of the negative pocket makes the upper part of the porin an unfavourable environment for glutamic acid as seen in the FES.

The structure corresponding to the deepest minimum for translocation of glutamic acid is shown in Figure S10. It is found in the region below the constriction region where both carboxyl groups strongly interact with the three residues of the basic ladder, R391, R389, and L375.

Benzoate being a small molecule, can access sterically hindered locations easier than glutamic acid and hence the FES is somewhat flat showing also some minima above the constriction region of the porin. The representative structures responsible for these minima are shown in Figure S11. In both cases, benzoate takes paths that are not accessible for larger molecules.
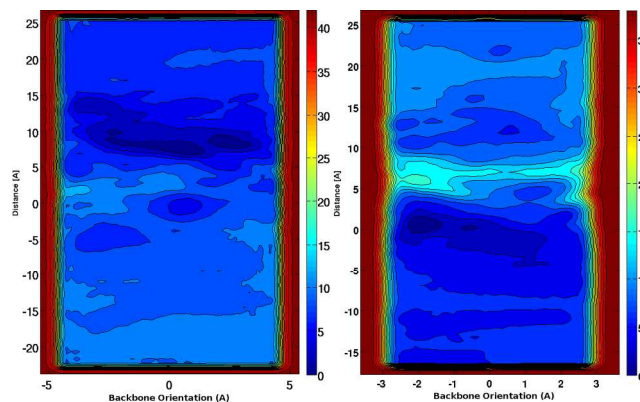
Fig. 11 of translocation of benzoate (left) and glutamic acid (right) through OprD.

Translocation of Neutral Substrates:

The reconstructed FES of neutral substrates glycine, leucine and serine through OprD are shown in Figure S12 in the SI. The energy barriers for the translocation were found to be 7.4 kcal /mol for glycine, 8.0 kcal/mol for leucine, and 10.6 kcal/mol for serine. The barriers for these amino acid are lower than those found for the translocation of the negative substrates investigated. The barrier for glycine and leucine, in particular, are comparable to those for the positive substrates. Serine has a slightly higher barrier compatible with the observation that it translocates following the secondary path B.

Paths of translocation:

Loops L3 and L7 spans across the lumen of OprD creating two possible paths for substrates translocation. Path A is located between these loops and the basic ladder, path B on the opposite side of the loops (Figure 2). Our analysis highlighted the preferred paths for translocation of the different substrates

investigated and results are summarized in Figure 12. Apart from the neutral histidine and serine, all the other amino acids share a similar path, between the negative pocket and the basic ladder. On the other hand, serine and the neutral form of histidine take the path through the loop L3. Benzoate, which is not shown in Figure 10, did not follow any specific path.
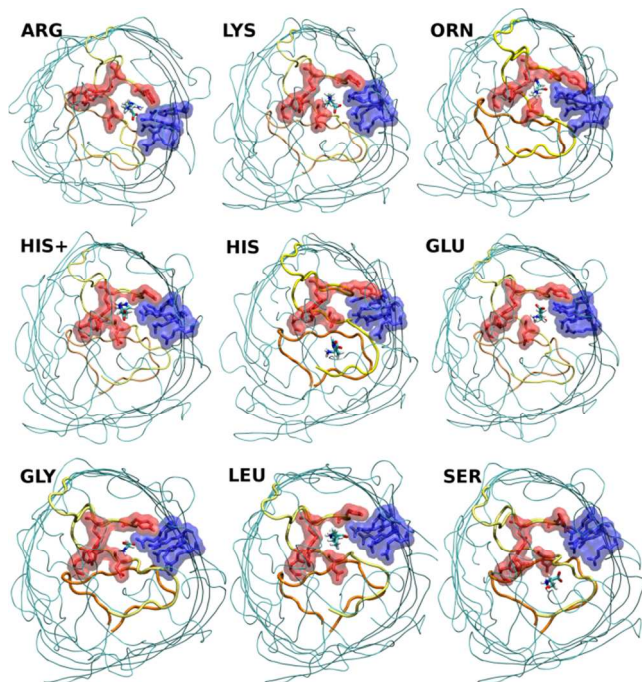
Fig. 12 Paths of translocation of substrates through OprD.

Conclusions

The simulations with external electric field were executed to pinpoint the possible open and closed state of OprD. Our studies show that the dynamics of loop L2 as the most important factor in opening and closing of the porin acting from the outside. Loop L2 works like a lid and, when closed, can hinder the admission of substrates/ions in the lumen. PCA shows that this is the most contributing motion in OprD. It also shows that the loop L2, L4 and L7 are indeed very flexible and mobile, providing a plausible explanation for being not resolved in the X-ray structure.

The internal loop L3 also plays an important role as seen in the electrophysiology simulations. Truncation of this loop increases the available area in the constriction region and in path A, leading to a two-fold increase in conductance. On the other hand, increasing the available area in path B (R131G mutation) does not significantly affect conductance. This implies that path A is much more important than path B for the translocation process through OprD. The negative pocket just above the constriction region of path A hinders the translocation of anions but favours the passage of cations. For this reason OprD showed a remarkable preference for cations in all our simulations. At pH 5, the overall negative charge of the protein is reduced, especially in the constriction region and hence, the anions current increases.

We can see the effect of paths in the translocation process of substrates. The electrostatics of the constriction region play a fundamental role not only in ions conductivity and selectivity, but

can be also clearly discerned for the translocation of molecular substrates. Path A is strikingly polar in nature as the basic ladder and the negative pocket face each other on opposite sides of the lumen. This effective charges segregation should generate an electric field probably strong enough to direct the orientation of charged and zwitterionic substrates in the constriction region. This existence of a strong transverse electric field in the constriction region of a general channel is responsible of strong ordering of water dipoles, as reported very recently in a study by our group.[38] Depending on the molecular charge distribution, this intrinsic porin's feature might facilitate or hinder the overall translocation process. Negatively charged molecules (benzoate and glutamic acid), has to cross the electrostatically unfavourable negative pocket before entering the eyelet region, giving rise to higher energy barriers. Positively charged molecules, on the other hand, can favourably interact with the residues comprising the negative pocket, ameliorating the energetics of their translocation across the constriction region. The free energy surfaces show that all the positively charged molecules have deep minima in the negative pocket. While the charged molecules show clear preference for path A, the neutral molecules do not have such specificity. They translocate both via path A (glycine, leucine) or B (neutral histidine, serine). The choice of path B gives rise to a higher barrier for translocation. The major factor controlling the path B is the salt bridge between R131 and D295. In order to open this path this salt bridge has to be broken, contributing to the relatively higher barrier for translocation.

In conclusion, the OprD shows, differently from other channels, a remarkable dynamics of both internal and external loops as well as a strong interplay among them, which is strictly related to the channel open and closed states. This is reflected by a rich diversity with respect to transport properties of ions and substrates that we quantified here using molecular dynamics simulations.

Notes and references

[a] Department of Physics, University of Cagliari, S.P. Monserrato-Sestu km 0.700, I-09042 Monserrato (CA), Italy. Fax: +39-070-6753191; Tel: +39-070-6754933; E-mail: matteo.ceccarelli@dsf.unica.it
[b] Department of Biomedical Sciences, University of Cagliari, S.P. Monserrato-Sestu km 0.700, I-09042 Monserrato (CA), Italy.
† Electronic Supplementary Information (ESI) available: Detailed figures of the mutations, current-voltage characteristics, details of the salt-bridge interactions, chemical structures of the substrates used, FESs, the structures corrsponding to them, and the convergence parameters can be found in the ESI. See DOI: 10.1039/b000000x/

1. D. J. Hoban, D. J. Biedenbach, A. H. Mutnick and R. N. Jones, *Diagnostic Microbiology and Infectious Disease*, 2003, **45**, 279-285.
2. E. F. Keen Iii, B. J. Robinson, D. R. Hospenthal, W. K. Aldous, S. E. Wolf, K. K. Chung and C. K. Murray, *Burns*, 2009, **36**, 461-468.
3. Q.-T. Tran, K. R. Mahendran, E. Hajjar, M. Ceccarelli, A. Davin-Regli, M. Winterhalter, H. Weingart and J.-M. Pages, *Journal of Biological Chemistry*, 2010, **285**, 32273-32281.
4. E. Eren, J. Parkin, A. Adelanwa, B. Cheneke, L. Movileanu, S. Khalid and B. van den Berg, *Journal of Biological Chemistry*, 2013, **288**, 12042-12053.
5. E. Eren, J. Vijayaraghavan, J. Liu, B. R. Cheneke, D. S. Touw, B. W. Lepore, M. Indic, L. Movileanu and B. Van den Berg, *PLoS Biology*, 2012, **10**, e1001242.
6. J. M. Pages, C. E. James and M. Winterhalter, *Nature Reviews Microbiology*, 2008, **6**, 893-903.
7. S. Kojima and H. Nikaido, *Proceedings of the National Academy of Sciences*, 2013, **110**, E2629-E2634.
8. M. Winterhalter and M. Ceccarelli, *European Journal of Pharmaceutics and Biopharmaceutics*, 2015.
9. C. Danelon, E. M. Nestorovich, M. Winterhalter, M. Ceccarelli and S. M. Bezrukov, *Biophysical Journal*, 2006, **90**, 1617-1627.
10. D. M. Livermore, *Journal of Antimicrobial Chemotherapy*, 1992, **29**, 609-613.
11. J. Trias and H. Nikaido, *Antimicrobial Agents and Chemotherapy*, 1990, **34**, 52-57.
12. J. Trias and H. Nikaido, *Journal of Biological Chemistry*, 1990, **265**, 15680-15684.
13. H. Huang and R. E. Hancock, *Journal of Bacteriology*, 1996, **178**, 3085-3090.
14. J. Parkin and S. Khalid, *Biophysical Journal*, 2014, **107**, 1853-1861.
15. Vincent M. Isabella, Arthur J. Campbell, J. Manchester, M. Sylvester, Asha S. Nayar, Keith E. Ferguson, R. Tommasi and Alita A. Miller, *Chemistry & Biology*, 2015, **22**, 535-547.
16. S. Biswas, M. M. Mohammad, D. R. Patel, L. Movileanu and B. van den Berg, *Nature Structural & Molecular Biology*, 2007, **14**, 1108-1109.
17. S. Tamber and R. E. W. Hancock, *FEMS Microbiology Letters*, 2006, **260**, 23-29.
18. S. Tamber, M. M. Ochs and R. E. W. Hancock, *Journal of Bacteriology*, 2006, **188**, 45-54.
19. G. D. Wright, *Chemistry & Biology*, 2012, **19**, 3-10.
20. D. J. Payne, M. N. Gwynn, D. J. Holmes and D. L. Pompliano, *Nature Reviews Drug Discovery*, 2007, **6**, 29-40.
21. K. Lewis, *Nature Reviews Drug Discovery*, 2013, **12**, 371-387.
22. H. Lou, M. Chen, S. S. Black, S. R. Bushell, M. Ceccarelli, T. Mach, K. Beis, A. S. Low, V. A. Bamford and I. R. Booth, *PLoS One*, 2011, **6**, e25825.
23. B. Webb and A. Sali, in *Current Protocols in Bioinformatics*, John Wiley & Sons, Inc.2002, pp. 5.6. 1-5.6. 30.
24. K. Lindorff-Larsen, S. Piana, K. Palmo, P. Maragakis, J. L. Klepeis, R. O. Dror and D. E. Shaw, *Proteins: Structure, Function, and Bioinformatics*, 2010, **78**, 1950-1958.
25. W. L. Jorgensen, J. Chandrasekhar, J. D. Madura, R. W. Impey and M. L. Klein, *Journal of Chemical Physics*, 1983, **79**, 926-935.
26. C. J. Dickson, L. Rosso, R. M. Betz, R. C. Walker and I. R. Gould, *Soft Matter*, 2012, **8**, 9617-9627.
27. M. J. Harvey, G. Giupponi and G. D. Fabritiis, *Journal of Chemical Theory and Computation*, 2009, **5**, 1632-1639.
28. T. Darden, D. York and L. Pedersen, *Journal of Chemical Physics*, 1993, **98**, 10089-10092.
29. S. F. Epp, T. Köhler, P. Plesiat, M. Michea-Hamzehpour, J. Frey and J.-C. Pechere, *Antimicrobial Agents and Chemotherapy*, 2001, **45**, 1780-1787.
30. M. Rostkowski, M. H. M. Olsson, C. R. Sondergaard and J. H. Jensen, *BMC Structural Biology*, 2011, **11**.
31. X. Daura, K. Gademann, B. Jaun, D. Seebach, W. F. van Gunsteren and A. E. Mark, *Angewandte Chemie International Edition*, 1999, **38**, 236-240.
32. A. AMADEI, A. LINSSEN and H. BERENDSEN, *Proteins-Structure Function and Genetics*, 1993, **17**, 412-425.
33. A. Amadei, A. Linssen, B. deGroot, D. vanAalten and H. Berendsen, *Journal of Biomolecular Structure & Dynamics*, 1996, **13**, 615-625.
34. R. Verma, U. Schwaneberg and D. Roccatano, *Journal of Chemical Theory and Computation*, 2013, **9**, 96-105.
35. M. Bonomi, D. Branduardi, G. Bussi, C. Camilloni, D. Provasi, P. Raiteri, D. Donadio, F. Marinelli, F. Pietrucci and R. A. Broglia, *Computer Physics Communications*, 2009, **180**, 1961-1972.
36. A. Barducci, G. Bussi and M. Parrinello, *Physical Review Letters*, 2008, **100**, 020603.
37. P. Raiteri, A. Laio, F. L. Gervasio, C. Micheletti and M. Parrinello, *Journal of Physical Chemistry B*, 2006, **110**, 3533-3539.
38. S. Acosta-Gutierrez, M. Scorciapino, I. Bodrenko and M. Ceccarelli, *Journal of Physical Chemistry Letters*, 2015, **6**, 1807-1812.